Measurement of the Deeply Virtual Neutral Pion Electroproduction Cross Section at the Thomas Jefferson National Accelerator Facility at 10.6 GeV

by

Robert Johnston

Submitted to the Department of Physics
in partial fulfillment of the requirements for the degree of

Interdisciplinary PhD in Physics and Statistics

at the

MASSACHUSETTS INSTITUTE OF TECHNOLOGY

June 2023

Author . . . .
Department of Physics
May 5, 2023

Certified by . . . .
Richard Milner
Professor of Physics
Thesis Supervisor

Accepted by . . . .
Lindley Winslow
Associate Department Head of Physics

Measurement of the Deeply Virtual Neutral Pion Electroproduction Cross Section at the Thomas Jefferson National Accelerator Facility at 10.6 GeV

by

Robert Johnston

Submitted to the Department of Physics
on May 5, 2023, in partial fulfillment of the
requirements for the degree of
Interdisciplinary PhD in Physics and Statistics

Abstract

Deeply virtual exclusive reactions provide unique channels to study both transverse and longitudinal properties of the nucleon simultaneously, allowing for a 3D image of nucleon substructure. This presentation will discuss work towards extracting an absolute cross section for one such exclusive process, deeply virtual neutral pion production, using 10.6 GeV electron scattering data off a proton target from the CLAS12 experiment in Jefferson Lab Hall B . This measurement is important as exclusive meson production has unique access to the chiral odd GPDs, and is also a background for other exclusive processes such as DVCS, making the determination of this cross section crucial for other exclusive analyses.

Thesis Supervisor: Richard Milner
Title: Professor of Physics

Acknowledgments

To Be Completed.

Contents

List of Figures

List of Tables

List of Equations

Chapter 1

Introduction

People have tried to understand the nature of the world around us for millennia, with discerning the structure of matter being a central effort in this quest. Famously, the Greek philosophers Leucippus and Democritus ($\sim$ 5th century BCE) are credited with the concept of "atomism" - the belief that matter is composed of tiny indivisible particles called atoms (from the Greek $\alpha\tau o\mu o\sigma$, roughly translating to "uncuttable" [1]. Even further back, there are Indian records from as early as the 8th century BCE conceptualizing the world as being built from tiny fundamental particles [2].

Scientific progress on this front stalled until the early 1800s, when chemists explored how different elements combined in to form compounds in specific, repeatable, small integer ratios. John Dalton formulated this idea as the Law of Multiple Proportions, which paved the way for early scientific atomic theory [3]. In 1897, J.J. Thomson discovered the first subatomic particle, the electron, by studying cathode rays[4]. Accordingly, he devised a model of the atom which had electrons embedded in a ball of positively charged material, called the Thomson, or Plum Pudding, Model[5].
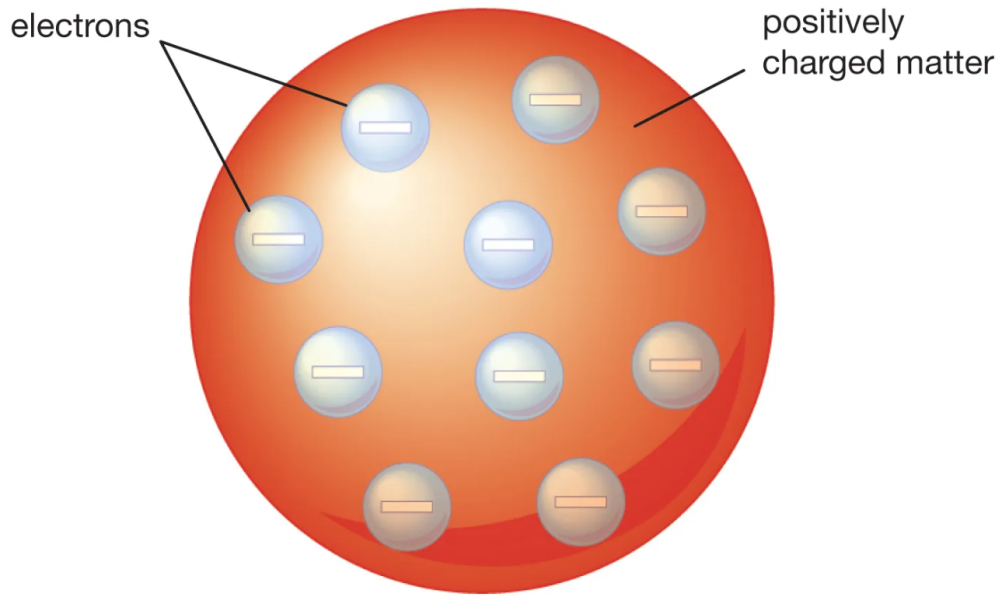
Figure 1-1: J.J. Thomson's Plum Pudding Model of the atom [6]

With the idea that the atom was a composite object, scientist began experimentation to study its exact structure. This was the start of what has been the 120 years of particle scattering studies to probe first atomic, then nuclear structure.

The rest of this chapter details the findings of previous scattering experiments and provides a background on Generalized Parton Distributions and Deeply Virtual Exclusive Processes, the topic of this work. Chapter 2 describes the experimental setup of the CLAS12 detector and data taking conditions. Chapter 3 discusses data analysis procedures to reconstruct particles and classify events from detector level information. Simulations and computational pipelines for this work are presented in chapter 4. The analysis procedure for combining experimental and simulated data into a differential cross section with correction factors is discussed in chapter 5. Chapter 6 displays and discusses results and uncertainties. Chapter 7 summarizes

this work and lays a path for finalizing the measurement. The appendicies include numerous technical details and supplemental plots.

1.1 Exploring Structure through Scattering

The typical length scales for atoms and nucleons are 0.1 nm which is far smaller than the wavelength of human-visible light ($\sim$ 500 nm). As such, atomic and nuclear structure must be explored by forcing some interaction and then inferring the structure from the observed results. Thomson's atomic model was famously tested in the early 1900s by Ernest Rutherford's research group, wherein α particles were fired at thin metal targets, and the scattering behaviour was observed [7] [8].

The results were not consistent with Thomson's model, but instead indicated that there was a very small, dense, positively charged nucleus at the center of every atom. Further experiments by Rutherford would lead to the discovery of the proton around 1920 [9]. Puzzles about the nucleus remained, including a consistent description of isotopes, until 12 years later when James Chadwick suggested the existence of the neutron [10]. With electrons and the two nucleons discovered, it seemed as though the indivisible constituents of the atom were finally realized, but future experiments showed a much more complex, sub-nuclear structure.

1.1.1 Scattering at Different Resolution Scales

The diffraction limit for microscopic (compared to telescopic) systems can be approximated by equation 1.1, where n is the index of refraction, θ is a measure of the device aperture, λ is the wavelength of the probe, and d is the minimum resolvable length scale. Thus, the wavelength of a probe sets a fundamental lower limit on

the achievable resolution of a microscopic imaging system - roughly, at small enough distances, the probe's waves interfer, prohibiting resolution at or below that scale.

$$d = \frac{\lambda}{2n \sin \theta} \tag{1.1}$$

For visible light microscope systems, $\lambda \sim 500$ nm, and so the minimum resolvable feature size is approximately $d \sim 250$ nm. Techniques exist to extend the resolution size by approximately an order of magnitude, e.g. expansion microscopy [11] or Near-Field Scanning Optical Microscopy [12], but non-visible-light probes are needed for scales below ~ 10 nm.

In particular, the de Broglie relationship 1.2 [13] states that the wavelength λ of a particle is inversely proportional to its momentum p, with h being Planck's constant.

$$\lambda = \frac{h}{p} \tag{1.2}$$

With this relationship, we can see that by increasing a particle's momentum, its effective wavelength is reduced. This is the fundamental principle which allows electron microscopes to image matter at a resolution of ~ 10-0.1 nm [14], corresponding to electron momentums of ~ 1-100 keV. At this scale, viruses, cells, molecular structures, and even atoms can be imaged [15], with striking results commonly published online. Other probes could be used circumvent the diffraction limit, such as high energy (low-wavelength) photons or high momentum (low de Broglie wavelength) protons or neutrons, but electrons are an ideal candidate in this regime as they are easy to produce, steer, interact with, and detect.

To move beyond imaging at the atomic scale (~ 1 Å) to the nuclear scale (~ 1

fm) requires probes that are 100,000 times more powerful. Electrons are still an ideal probe due to their (apparent) lack of internal structure, but rather than a room sized microscope, an entire accelerator facility is needed to achieve high enough energies and luminosities for sub-nuclear scale resolution.

1.1.2 Elastic Scattering and Form Factors

Imaging with electrons (or other non-visible-light probes) at any energy scale is commonly understood in terms of scattering cross sections, σ, with dimensions of area and interpreted as the probability for a certain interaction to occur. Typical elastic scattering cross sections for transitions metals with 100 keV incident electrons as in electron microscopy are $\sim 10^{-22} m^2$ [15]. In contrast, the cross sections to be discussed in this thesis are on the order of tens of nanobarn ($10^{-36} m^2$), or 14 orders of magnitude smaller.
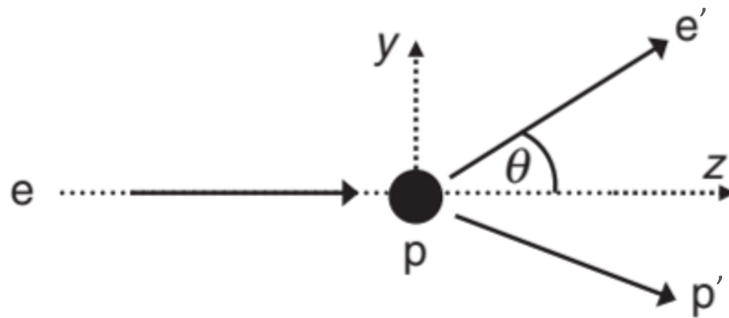

Figure 1-2: Elastic scattering diagram

The scattering cross section for a probe (such as an electron) incident on a target, can be calculated at lowest order by considering a fixed (no recoil), point-like (no structure), radially symmetric Coulomb potential (e.g., a proton) with a non-relativistic incident charged particle. The resulting equation was used by Ruther-

ford's group in the discovery of the nucleus, and for an electron beam of energy E_{beam} is given by Eq. 1.3, where α is the fine structure constant.

$$\frac{\theta}{2}(\frac{d\sigma}{d\Omega})_{Ruth} = \frac{\alpha^2}{16E_{beam}^2 \sin^4(\theta/2)} \tag{1.3}$$

To probe smaller resolution scales, it is necessary to increase the energy of the beam, and eventually the probe must be treated relativistically. This correction term is provided by the Mott scattering cross section, given by Eq. 1.4, which still assumes a fixed, point-like target, with only Coulomb interactions.

$$(\frac{d\sigma}{d\Omega})_{Mott} = \frac{\alpha^2}{4E^2 \sin^4(\theta/2)} \cos^2 \frac{\theta}{2} = \left(\frac{\alpha}{2E \sin^2(\theta/2)} \cos \frac{\theta}{2} \right)^2 = 4\cos^2 \frac{\theta}{2}(\frac{d\sigma}{d\Omega})_{Ruth} \tag{1.4}$$

At higher incident electron energies (and thus finer spatial resolutions), the proton's finite size must be accounted for, as well as the momentum transferred to it. The tree-level Feynman diagram for elastic electron-proton scattering is show in in Fig. 1.1.2. The incoming electron e exchanges a virtual photon with the proton p, resulting in a momentum transfer of $q = p_{e'} - p_e$.
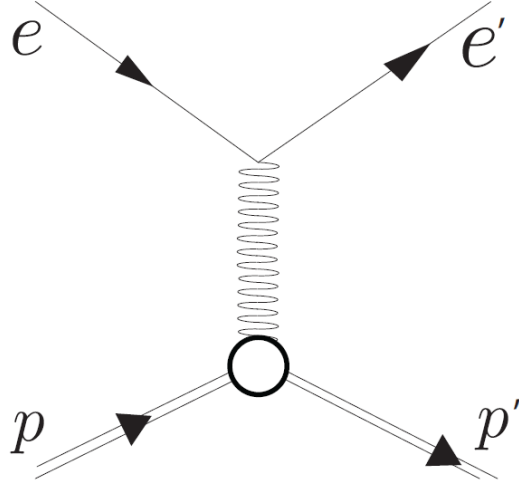
Figure 1-3: Tree-level elastic scattering Feynman diagram

The momentum transfer q sets the resolution scale for these processes, but it is convenient to work with the negative square of this value, defined as $Q^2 = -q^2$. With this term, we can express the relativistic differential cross section for the scattering of electrons off a resting, point-like proton as in Eq. 1.5, where m_p is the mass of the proton.

$$\frac{d\sigma}{d\Omega} = \frac{\alpha^2}{4E_{beam}^2 \sin^4\left(\theta/2\right)} \frac{E_{e'}}{E_{beam}} (\cos^2\frac{\theta}{2} + \frac{Q^2}{2m_p^2} \sin\frac{\theta}{2}^2) \qquad (1.5)$$

Compared with Mott Scattering, there are two differences in this formula: The $\frac{E_{e'}}{E_{beam}}$ term in the scattering cross section comes from the electron losing energy to the proton's final state kinetic energy (no longer fixed), and the term proportional to $\sin^2(\theta/2)$ is due to a purely magnetic spin-spin interaction.

If the proton were a point, then Eq. 1.5 would agree with experiment for all

17

electron scattering energies. Instead, deviations are observed as we increase the beam energy. To account for this structure, we need to include two form factors, $G_E(Q^2)$ - related to the distribution of charge, and $G_M(Q^2)$, related to the distribution of the magnetic moment inside the proton. In the low-Q^2 limit, these form factors are the Fourier transforms of the charge an magnetic moment distributions as in Eq. 1.6 and 1.7, reducing to the charge and the magnetic moment of the proton in the $Q^2 = 0$ limit.

$$G_E(Q^2) \approx G_E(q^2) = \int e^{iq \cdot r} \rho(r) d^3 r \qquad G_E(0) = \int \rho(r) d^3 r = 1 \qquad (1.6)$$

$$G_M(Q^2) \approx G_E(q^2) = \int e^{iq \cdot r} \mu(r) d^3 r \qquad G_M(0) = \int \mu(r) d^3 r = 2.79 \qquad (1.7)$$

Including these form factors in our cross section gives us the full elastic scattering cross section, as shown in Eq. 1.8.

$$\frac{d\sigma}{d\Omega} = \frac{\alpha^2}{4E_1^2 \sin^4 (\theta/2)} \frac{E_3}{E_1} \left(\frac{G_E^2 + \tau G_M^2}{1 + \tau} \cos^2 \frac{\theta}{2} + 2\tau G_M^2 \frac{Q^2}{2m_p^2} \sin^2(\frac{\theta}{2}) \right) \qquad (1.8)$$
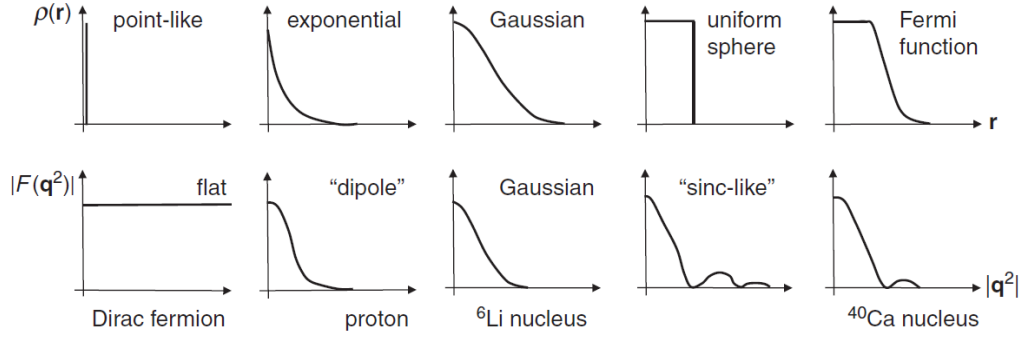
Where $\tau = \frac{Q^2}{4m_p^2}$.

Figure 1-4: Samples of charge distributions and their corresponding form factors $F(\mathbf{q}^2)$, from [16]

By the 1960s, elastic scattering had been studied sufficiently well as to measure the proton form factors up to several GeV in Q^2. The observed results were consistent with a proton having a 'dipole' form factor, as shown in Fig. 1.1.2. Investigating proton structure at finer spatial resolutions requires increasing the beam energy, but eventually the the elastic scattering cross section becomes negligible and instead the interactions are sufficiently energetic so as to create additional particles.

1.1.3   Inelastic Scattering and Parton Distribution Functions

Elastic scattering can be defined as interactions where the target stays intact; specifically, the variable $W = p_p + q$ is the four-momentum of the outgoing struck target, where elastic scattering satisfies the condition $W^2 = m_p^2$. If W^2 m_p^2, we instead have inelastic scattering, written as ep→eX, where X stands for some outgoing hadronic system, as shown in the Feynman diagram in Fig. 1.1.3.

In general,

Since we remove the constraint that the mass of the final state is the proton mass, we now have one extra degree of freedom, i.e., we need 2 variables to describe
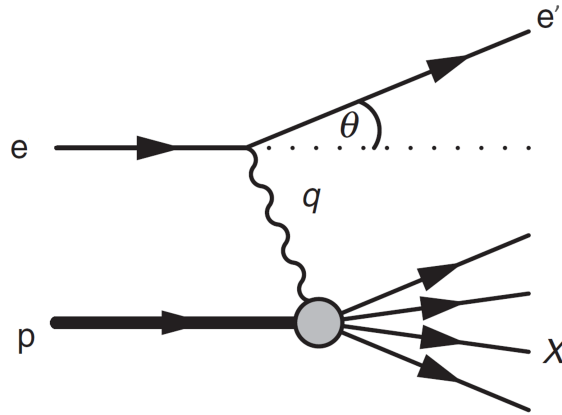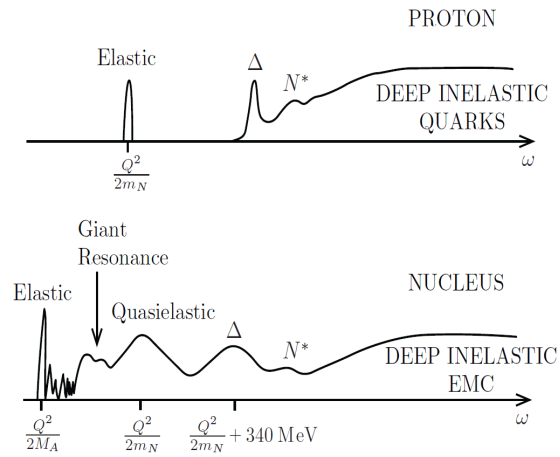
Figure 1-5: Diagram

Figure 1-6: Sketch of cross section as a function of electron energy transfer for inclusive electron scattering off a proton (top) and a nucleus (bottom), from [17]

inelastic scattering. These are usually Bjorken X x_B and the 4-momentum transfer of the virtual photon Q^2.

x_B is a measure of elasticity - 1 for elastic scattering. Also, is the fraction of proton momentum carried by the struck quark in the infinite momentum frame. Think of Xb as the ratio of momentum transfer to energy transfer.

$$x = \frac{Q^2}{2p_2 \cdot q} = \frac{Q^2}{Q^2 + W^2 - m_p^2} \tag{1.9}$$

The Deep Inelastic Scattering regime is defined by kinematics as Q^2 1 GeV^2 and W^2 4 GeV^2

Derivation of infinite momentum frame Bjorken x. Take quark to have momentum fraction ξ of proton's total momentum,i.e. $p_q = \xi p_2$:

Inf. Mom. frame - neglect proton mass so $p_2 = E_2$, neglect all transverse momenta:

Struck quark 4-momenta: $p_q = \xi p_2 = (\xi E_2, \xi E_2, 0, 0)$

4-momenta of quark after interaction: $(p_q + q) = (\xi p_2 + q)$

Square the 4-momenta $(\xi p_2 + q)^2 = \xi^2 p_2^2 + q^2 + 2\xi p_2 \cdot q = m_q^2$

Continue, noting $p_q = \xi p_2$: $m_q^2 = p_q^2 - Q^2 + 2\xi p_2 \cdot q$

Since $p_q^2 = m_q^2$, we have: $m_q^2 = m_q^2 - Q^2 + 2\xi p_2 \cdot q$

So $0 = -Q^2 + 2\xi p_2 \cdot q \longrightarrow \xi = \frac{Q^2}{2p_2 \cdot q} = x_B$

y is a measure of the inelasticity of the scattering, it is the fractional energy lost by the electron in the scattering process (second equality is true where proton is at rest). 0 is for perfectly elastic, 1 is for entirely inelastic.

$$y = \frac{p_2 \cdot q}{p_2 \cdot p_1} = 1 - \frac{E_3}{E_1} \tag{1.10}$$

We get quark PDFs from the F2 structure function. How do we get gluon PDFs? Can we probe the gluon directly? Does it couple to the photon? No! We assume QCD evolution equations (e.g. DGLAP) and gluon dist comes out.

W is the four momenta of the final state system that started with the proton, W = q + p_2. It is useful as $W^2 = m_p^2 - Q^2 + 2p_2 \cdot q$

To describe further proton sub-structure, we need to introduce structure functions, $F_1(x, Q^2)$ - purely magnetic, and $F_2(x, Q^2)$. For DIS where $Q^2 \gg m_p^2 y^2$, we have the following cross section formula:

$$\frac{d^2\sigma}{dx\,dQ^2} \approx \frac{4\pi\alpha^2}{Q^4}\left[(1-y)\frac{F_2(x, Q^2)}{x} + y^2 F_1(x, Q^2)\right].$$

Figure 1-7: General DIS cross section

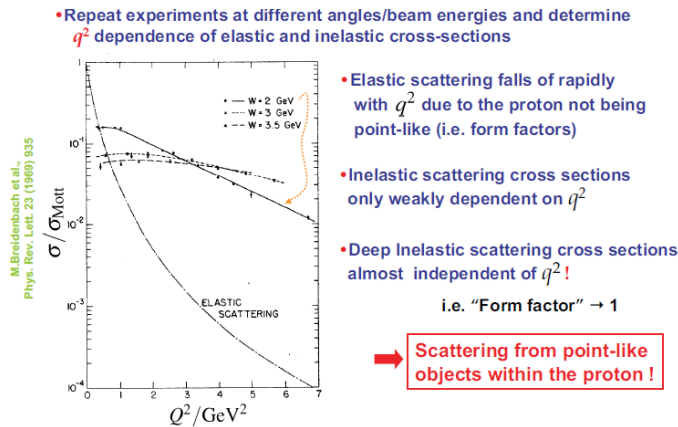In DIS, we observe Bjorken scaling and Callan-Gross

Figure 1-8: Early Bjorken Scaling Example

After performing DIS measurements at SLAC with electron energies between 5 and 20 GeV on liquid hydrogen, using a movable spectrometer over various angles, showed two important results:

Bjorken Scaling where F_1 and F_2 are basically flat with respect to Q^2, and thus are independent of Q^2, indicating that we are scattering off point-like constituents inside the proton.

Callan Gross Relation where $F_2 = 2xF_1$, a relation which can be explained by assuming the underlying process is actually elastic scattering off of point-like spin-half constituents inside the prton (quarks).

These describe the distribution of quarks within the nucleon. Describes the momentum fraction distribution of quarks. For example:

$u^p(x)dx$

Represents the number of up-quarks within the proton with momentum fraction between x and dx. The functional forms of the PDFs are not a-priori known. Some potential PDFs could be as shown below:
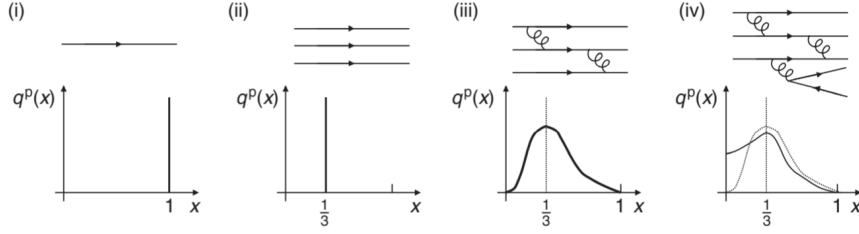

Figure 1-9: Potentail PDFs

(i) - if the proton consisted of a single quark

(ii) - if the proton had 3 static quarks

(iii) - quarks interacting and Heisenberg uncertainty (momentum smearing)

(iv) - interacting quarks with higher order diagrams - gluons produced, so enhances low x part of PDF

We can access these distributions experimentally as the parton model predicts the the cross section for elastic scattering off of quarks with charge Q_i and momentum fraction in the range of x to x + dx as:

$$\frac{\mathrm{d}^2\sigma}{\mathrm{d}Q^2} = \frac{4\pi\alpha^2}{Q^4}\left[(1-y) + \frac{y^2}{2}\right] \times Q_i^2 q_i^{\mathrm{p}}(x)\,\delta x\,,$$

Figure 1-10: Quark scattering cross section

So then the cross section summing over all quark flavours is:

$$\frac{\mathrm{d}^2\sigma^{\mathrm{ep}}}{\mathrm{d}x\,\mathrm{d}Q^2} = \frac{4\pi\alpha^2}{Q^4}\left[(1-y)+\frac{y^2}{2}\right]\sum_i Q_i^2 q_i^{\mathrm{p}}(x).$$

Figure 1-11: Quark PDF - cross section relation

and comparing it with the general expression for DIS cross section:

$$\frac{\mathrm{d}^2\sigma}{\mathrm{d}x\mathrm{d}Q^2} = \frac{4\pi\alpha^2}{Q^4}\left[(1-y)\frac{F_2^{\mathrm{ep}}(x,Q^2)}{x} + y^2 F_1^{\mathrm{ep}}(x,Q^2)\right],$$

Figure 1-12: General DIS cross section

We see we can get the relation:

$$F_2^{\mathrm{ep}}(x,Q^2) = 2xF_1^{\mathrm{ep}}(x,Q^2) = x\sum_i Q_i^2 q_i^{\mathrm{p}}(x).$$

Figure 1-13: Structure function - quark PDF relatio

For an explicit example, we have (neglecting heavier quarks, which have smaller contributions):

$$F_2^{\mathrm{ep}}(x) = x\sum_i Q_i^2 q_i^{\mathrm{p}}(x) \approx x\left(\frac{4}{9}u^{\mathrm{p}}(x) + \frac{1}{9}d^{\mathrm{p}}(x) + \frac{4}{9}\bar{u}^{\mathrm{p}}(x) + \frac{1}{9}\bar{d}^{\mathrm{p}}(x)\right),$$

Figure 1-14: Up and Down quark contributions to structure functions

Note that the parton model predicts both Bjorken scaling and the Callan Gross relation. Importantly, because QCD is hard, the PDFs cannot be calculated from perterbation theroy, and must be measured in DIS. We can integrate the PDFs to

determine the total momentum fraction of the proton carried by each flavour of quark, as:

$$f_{\mathrm{u}} = \int_0^1 [xu(x) + x\bar{u}(x)]\,\mathrm{d}x \quad \text{and} \quad f_{\mathrm{d}} = \int_0^1 [xd(x) + x\bar{d}(x)]\,\mathrm{d}x \,.$$

Figure 1-15: Total quark momentum fractions

Doing this after DIS measurements yields $f_u = 0.36$ and $f_d = 0.18$, so the u and d quarks only carry about half of the total momentum of the proton. The rest is carried by gluons, which do not interact in QED ep scattering.

Structure functions were studied in great detail (one million DIS events at Q^2 greater than 200 GeV^2 - kinematic range was up to $Q^2 = 20,000 GeV^2$ and $x < 0.0001$. Q^2 and x were determined solely by precisely measuring the scattering angle and energy of the electron.
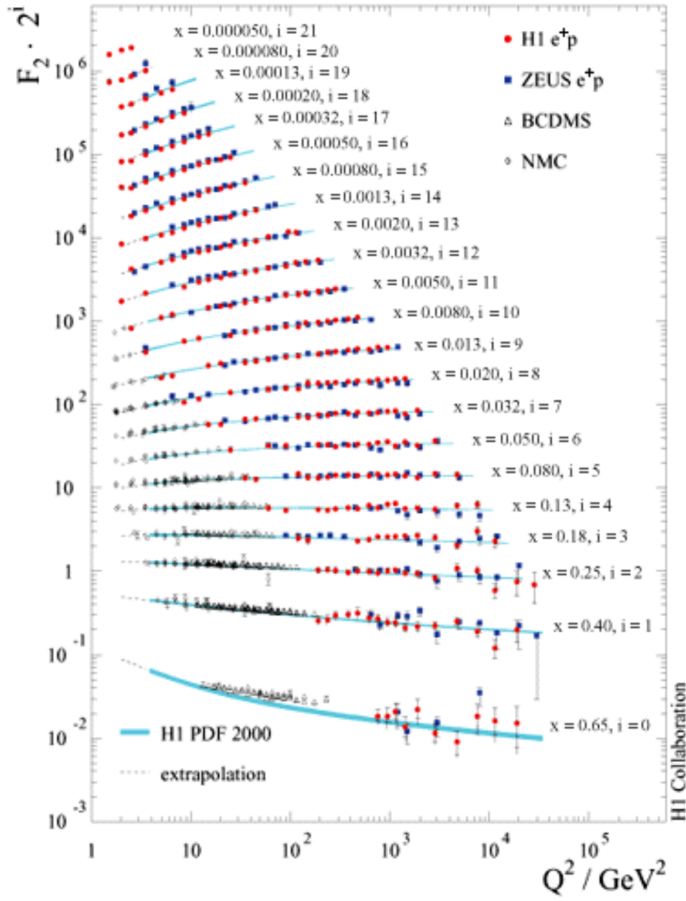
FIG. 2: Structure function F_2 as a function of Q^2 based on HERA-I measurements of H1 [2, 3] and ZEUS [4] collaboration compared to results from fixed target experiments BCDMS [5] and NMC [6].

Figure 1-16: HERA structure functions

2 important takeaways:

1- Bjorken scaling holds up to $Q^2 = 20,000$ GeV^2, implying that quarks are point like up to scales of at least 10^{-18}m.

2- **Scaling violations:**

At medium X, we are independent of Q2, indicating we have quarks. At high x, the F_2 structure function decreases at high x, and increases at low x, with increasing Q^2. More specifically, imagine measuring the F_2 structure function across x at a certain Q^2. Now measure again at a higher Q^2. You will see the curve is shifted higher at low x, and lower at high x:
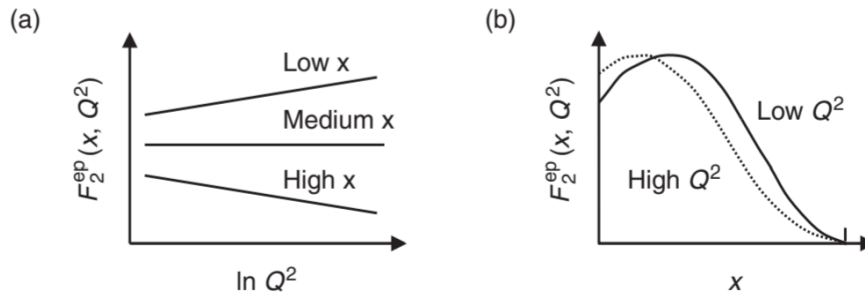

Figure 1-17: Explaination of Scaling Violations

This is indicative of the fact that at higher Q^2, the proton has a greater fraction of low x quarks. I.e., at low Q^2 we do not "see" the low-x quarks, but as we increase our resolving power, we do.

N.b. - we cannot measure the gluon PDFs, but can model them with QCD parton evolution equations such as DGLAP or BFKL.

Finally, we include a proton PDF at $Q^2 = 10$ GeV^2 and at 10^4 GeV^2. (note - on a semilog plot!)
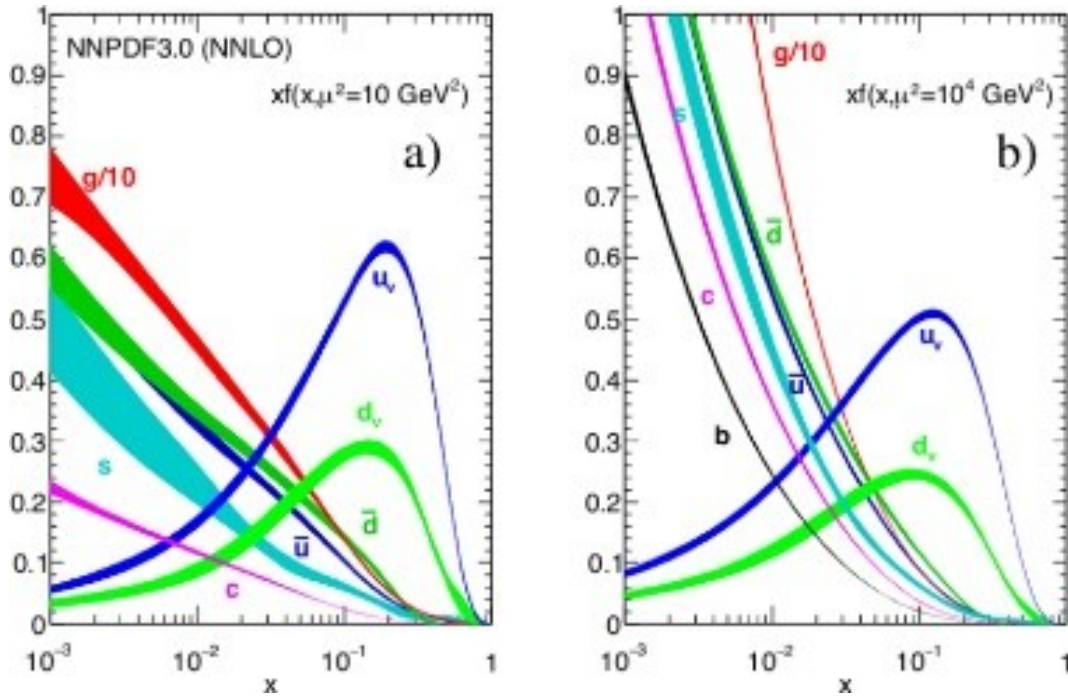
Figure 1-18: PDFs at two different Q^2 values

PDFs allow for a 1 dimensional picture of the inner workings of a proton - proton femtography. Even more informaiton can be gleaned from scattering reactions. In particular, efforts are now directed towards so called nuclear tomography - 3D imaging of nucleon structure.

Bibliography

[1] C.C.W. Taylor, *The atomists, Leucippus and Democritus: fragments, a text and translation with a commentary* (University of Toronto Press, 1999), ISBN 0-8020-4390-9.

[2] Thomas McEvilley, *THe Shape of Ancient Thought: Comparative Studies in Greek and Indian Philosophies* (Allworth Press, New York, 2002), ISBN 978-0-8020-4390-0.

[3] T. E. o. E. Britannica, *law of multiple proportions* (2010), URL https://www.britannica.com/science/law-of-multiple-proportions.

[4] J. Thomson, The Poular Science Monthly pp. 323–325 (1901), URL https://books.google.com/books?id=3CMDAAAAMBAJ&pg=PA323#v=onepage&q&f=false.

[5] Jaume Navarro, *A History of the Electron: J.J. and G.P. Thomson* (Cambridge University Press, 1995), ISBN 978-1-107-00522-8.

[6] T. E. o. E. Britannica, *"Thomson atomic model"* (2023), URL https://www.britannica.com/science/Thomson-atomic-model.

[7] H. Geiger and E. Marsden, Proceedings of the Royal Society of London Series A **82**, 495 (1909).

[8] E. Rutherford, Philosophical Magazine Series 6 **21**, 669 (1911).

[9] E. Rutherford, Philosophical Magazine Series 6 **37**, 581 (1919), URL https://www.tandfonline.com/doi/abs/10.1080/14786431003659230.

[10] J. Chadwick, Nature **129**, 312 (1932), ISSN 0028-0836.

[11] F. Chen, P. W. Tillberg, and E. S. Boyden, Science **347**, 543 (2015), ISSN 0036-8075, URL https://www.science.org/doi/10.1126/science.1260088.

[12] X. Ma, Q. Liu, N. Yu, D. Xu, S. Kim, Z. Liu, K. Jiang, B. M. Wong, R. Yan, and M. Liu, Nature Communications **12**, 6868 (2021), ISSN 2041-1723.

[13] L. d. Broglie, The London, Edinburgh, and Dublin Philosophical Magazine and Journal of Science **47**, 446 (1924), ISSN 1941-5982, URL https://www.tandfonline.com/doi/full/10.1080/14786442408634378?scroll=top&needAccess=true&role=tab.

[14] L. E. Franken, K. Grünewald, E. J. Boekema, and M. C. A. Stuart, Small **16**, 1906198 (2020), ISSN 1613-6810, URL https://onlinelibrary.wiley.com/doi/full/10.1002/smll.201906198.

[15] D. B. Williams and C. B. Carter, *Transmission Electron Microscopy* (Springer US, Boston, MA, 2009), ISBN 978-0-387-76500-6, URL https://link.springer.com/book/10.1007/978-0-387-76501-3.

[16] M. Thomson, *Modern Particle Physics* (Cambridge University Press, 2013), ISBN 9781107034266.

[17] T. W. Donnelly, J. A. Formaggio, B. R. Holstein, R. G. Milner, and B. Surrow, *Foundations of Nuclear and Particle Physics* (Cambridge University Press, 2017), ISBN 9780521765114.

Appendix A

Full Cross Section Data

To be completed

Appendix B

BSA Cross Check

As an additional cross check, Bobby calculated a $DV\pi^0 P$ beam spin asymmetry and compared to Andrey Kim's results. This check will not comment on any acceptance, luminosity, or virtual photon flux factor calculations, but does validate exclusive event selection criteria. By examining figure B-1 we can see that agreement is reasonable, especially considering Bobby's calculation does not have sideband subtraction included.

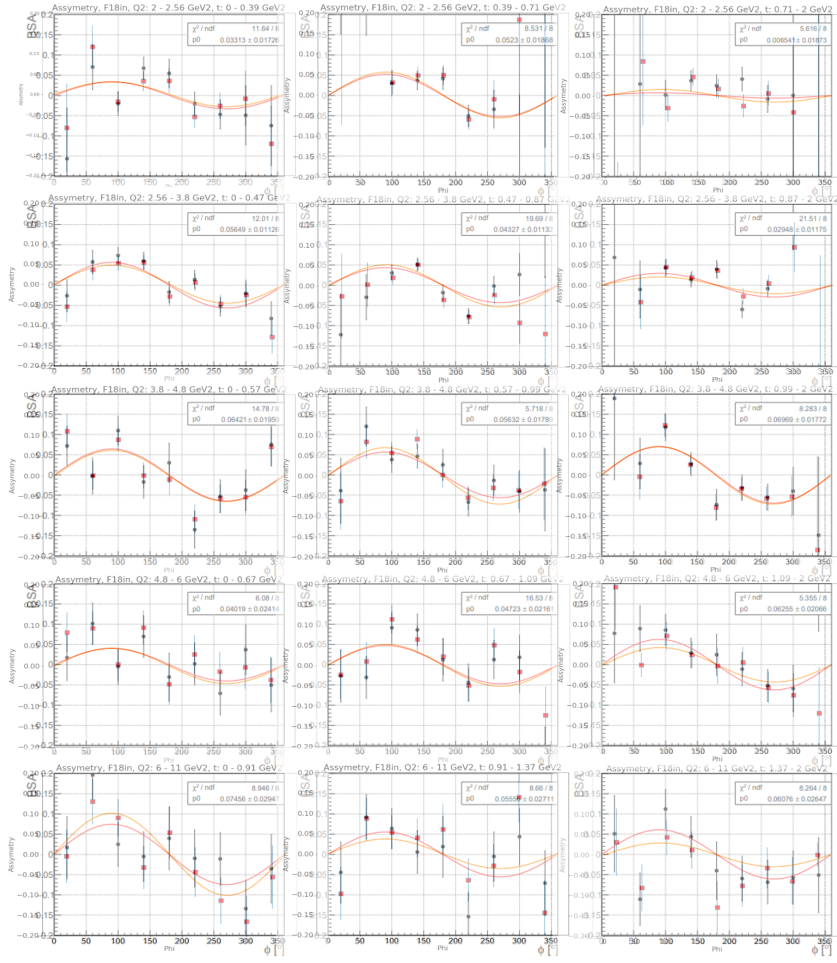Fig B-1 shows an overlay comparison of Andrey Kim's results (black datapoints, red fit line) and Bobby's results (red datapoints, orange fit line

Figure B-1: BSA Cross Check Results